Intercomparison of deep learning architectures for the prediction of precipitation fields

Noelia Otero and Pascal Horton

[1]Institute of Geography and Oeschger Centre for Climate Change Research, University of Bern, Bern, Switzerland

Abstract

In recent years, the use of deep learning methods has rapidly increased in many research fields. Similarly, they have become a powerful tool within the climate scientific community. Deep learning methods have been successfully applied for different tasks, such as identification of atmospheric patterns, weather extreme classification, or weather forecasting. However, due to the inherent complexity of the atmospheric processes, the ability of deep learning models to simulate natural processes, such as precipitation, is still challenging. Therefore, a thorough evaluation of their performance and robustness in predicting precipitation fields is still needed, especially for extreme precipitation events, which can be devastating in terms of infrastructure damage, economic losses, and even loss of life. In this study, we present a comprehensive evaluation of a set of deep learning architectures to realistically simulate precipitation, including heavy precipitation events (>95th percentile) and extreme events (>99th percentile) over the European domain. Moreover, we examine the optimal number of inputs based on the importance of the predictors derived from a layer-wise relevance propagation procedure. Among the architectures analyzed here, the U-Net network was found to be superior and outperformed the other networks to simulate precipitation events. Moreover, we found that a simplified version of the original U-Net with a single encoder-decoder level achieves similar skill scores as deeper versions for predicting precipitation extremes, significantly reducing overall complexity and computing resources.

Plain Language Summary

With the increasing success of machine learning methods in Earth Sciences, deep learning is becoming a promising tool for building data-driven models for meteorological applications. Yet, predicting extreme events, such as heavy rainfall, is still challenging. We present an intercomparison of deep learning models to assess the capability of different architectures to predict precipitation events.

1 Introduction

Predicting precipitation is challenging for numerical weather prediction (NWP) models. Precipitation involves complex microphysical processes that cannot be explicitly resolved in most models due to inadequate grid resolution and high computational requirements. Such processes are inferred from parametrization schemes, which are generally sources of parametric uncertainty (Bauer et al., 2015). NPW models solve numerically coupled partial differential equations subject to dynamic and thermodynamic laws that describe the atmospheric state (Schultz et al., 2021). Therefore, NPW models are computationally expensive.

A major concern relates to extreme precipitation events that are expected to change in intensity and frequency under a changing climate, leading to higher socio-economic impacts (Trenberth et al., 2003; Donat et al., 2016). The skill of climate models, or more specifically general circulation models (GCM), to predict extreme events is rather limited due to their lack of ability to represent mesoscale processes that require higher spatio-temporal resolutions (Gao & A., 2019). Regional climate models (RCM) can better represent topography and small-scale microphysical processes thanks to a higher spatial resolution (2–25 km) but are computationally expensive (Adewoyin et al., 2021). Alternatively, statistical downscaling techniques can establish relationships between large-scale variables (predictors) and the variable of interest (predictand) (Maraun et al., 2017).

With the rapid development of machine learning (ML) techniques, sophisticated deep learning (DL) models, and the availability of large data sets, there is an increasing interest in the weather and climate research community to tackle climate-related problems using ML. ML models can extract high-level feature representations from observed patterns and relate them to general meteorological situations. Moreover, ML models are computationally much cheaper than physically-based modeling of the physical processes responsible for precipitation. Recent studies have proposed different ML methods and DL architectures to predict precipitation at several time scales, including nowcasting, sub-seasonal, and seasonal forecast (Vandal et al., 2019; Hwang et al., 2019; Civitarese et al., 2021). These ML applications have shown promising results for predicting precipitation (Adewoyin et al., 2021).

Data-driven approaches have become very popular in many fields of natural sciences due to their ability to learn and efficiently represent underlying physical processes (Rasp et al., 2020). Several studies have shown the great potential of convolutional neuronal network (CNN) architectures to reproduce synoptic patterns (Chattopadhyay et al., 2020), weather extreme events (Liu et al., 2016), and provide weather forecasting (Weyn et al., 2019; Scher, 2018). In particular, precipitation forecasting has been the subject of DL studies that have proposed advanced network architectures that can outperform conventional forecast models (Rasp et al., 2020).

Previous works have used DL to predict extreme precipitation for spatially aggregated time series (Davenport & Diffenbaugh, 2021; Huang, 2022) or to predict high-resolution precipitation locally (i.e., statistical downscaling) (Adewoyin et al., 2021; Pan et al., 2019). However, the extreme values in the predicted precipitation fields over a larger domain have not yet been investigated enough nor improved. Therefore, this work aims to fill this gap by assessing the performance of existing DL models to predict spatial precipitation extremes. Building upon recent works, we present an intercomparison of DL architectures and assess their ability to predict extreme precipitation events over Europe. In addition, a baseline model was used to benchmark the performance of the selected DL architectures. The baseline consists in a random forest (RF) model (Breiman, 2001), a commonly used and robust algorithm that has been previously applied to predict precipitation (e.g., G. R. Hill A. J. Herman & S., 2022; A. J. Hill & S., 2022; Wolfensberger et al., 2021). While our primary focus is to test the model performance to capture precipitation extremes, we also examine the DL performance for precipitation estimates. Contrasting with most of the existing literature where the domain of interest focused on precipitation over the U.S. (e.g., Davenport & Diffenbaugh, 2021; Pan et al., 2019), here we present a model comparison over the European domain. The skills of the models are compared for the prediction of the spatial precipitation amount as well as for the spatial probability of exceedance of the 95th (i.e., heavy precipitation) and 99th (i.e., extreme precipitation) percentiles. In a second step, we conduct several experiments to assess the effect of the model depth. Furthermore, we apply a layer-wise relevance propagation (LWR) method to interpret the role of the different input features for heavy precipitation events and evaluate the optimal number of input data.

The rest of the paper is organized as follows: Section 2 discusses previous related work. The data and methods are introduced in Section 3. Section 4 shows the results and the main conclusions are summarized in Section 5.

2 Related works

Recently, many studies have proposed using sophisticated ML methods to improve precipitation estimates in various contexts, such as precipitation nowcasting (Ayzel et al., 2019) and post-processing of NWP precipitation output (Hess & Boers, 2022). This section reviews the most relevant studies closely related to our objectives and methodology.

Davenport and Diffenbaugh (2021) analyzed extreme precipitation days (above 95th percentile) over the U.S. Midwest and their links to large-scale atmospheric circulation patterns using a CNN with daily sea level pressure and geopotential height anomalies as input fields (Table 1). The model architecture consisted of two convolutional layers, each followed by a max-pooling layer, a dense 16-neuron layer, and a final classification layer of extreme and non-extreme precipitation days. The CNN showed high accuracy (91%) for the identification of extreme precipitation days, although some extreme events were not captured. The authors suggested that additional variables representing smaller-scale processes might improve the model performance. Moreover, due to the differences in the seasonal distribution of precipitation during extreme events, they pointed out the relevance of incorporating temporal information.

Building upon the work of Davenport and Diffenbaugh (2021), Huang (2022) proposed a self-attention augmented convolution mechanism for short-term extreme precipitation forecasting over the U.S. Midwest. The network consisted of two attention-augmented convolutional layers, a max-pooling, and a dropout layer. The proposed model outperformed classical convolutional models by 12%. However, a limitation to capturing some extreme events was acknowledged, likely due to localized processes for which additional information (e.g., variables) might be required.

Focusing on precipitation downscaling to point locations, Pan et al. (2019) proposed a CNN model as an alternative to parameterization schemes for numerical precipitation estimation. They built a CNN model based on convolutional and pooling layers using the geopotential height at several pressure levels and the total column water as inputs (at a 3-hourly time step; see Table 1). The extracted features were flattened and processed by two final dense layers. The authors tested the CNN in different locations across the U.S. and showed that the CNN outperformed the reanalysis precipitation products and classical statistical methods. However, the model underestimated large precipitation values.

Similarly, Shi (2020) evaluated the performance of ML methods, including CNNs, for statistical downscaling of extreme precipitation in three Asian regions. They compared two DL architectures, RaNet with three convolutional layers and five fully connected layers, and RxNet, a more complex model with 58 layers, including residual connections similar to the original Xception model (Chollet, 2017). The results showed that deep CNN with an intermediate-level complexity structure (e.g., RaNet) generally performed better than a more complex architecture (e.g., RxNet). Moreover, while the CNNs well captured the precipitation extremes in the subtropical regions, they performed poorly in the tropical regions, illustrating the challenge of representing extreme precipitation in certain regions.

Adewoyin et al. (2021) developed TRU-NET (Temporal Recurrent U-Net), a DL model based on a U-Net (Sect. 3.2.1) architecture and featuring a novel 2D cross attention mechanism to account for the spatio-temporal nature of weather processes. It relies on Convolutional Long Short-Term Memory (ConvLSTM) cells, more specifically Convolutional Gated Recurrent Units (ConvGRU). Their objective is to improve the prediction of high-resolution precipitation for climate models, which provide low-resolution outputs. They used 6 model fields as input, including mean sea level pressure, geopotential height, specific humidity, water vapor, and wind components (Table 1), at a 65 km spatial resolution and 6-hourly time step to predict precipitation over the UK at an 8.5 km resolution. The outputs are the rainfall probabilities and the rainfall values. The TRU-NET architecture captures the variability at different spatio-temporal scales through its 3-layers encoder: from six-hourly/8.5 km, to daily/34 km, and to weekly/136 km. They propose a Fused Temporal Cross Attention (FTCA) as a better aggregation strategy than averaging the six-hourly data to a daily time step. They show that TRU-NET outperforms other models, including U-Net, and conclude that this is due to its ability to use the temporal information present in weather data. However, they notice that TRU-NET under-predicts high precipitation events (> 20 mm/d).

Recently, Hess and Boers (2022) showed that a U-Net-based network, using NWP ensemble simulations as input features, captures well heavy rainfall events. They applied DL as a post-processing step to correct biases in the NWP-predicted rainfall. They proposed a frequency-based weighting of the loss function that combines a continuously weighted mean square error (MSE) with a multi-scale structural similarity measure, which improved the training for high values when using both metrics separately.

3 Data and Methods

3.1 Data

The input variables and the precipitation fields were retrieved from the ERA5 (Hersbach et al., 2020) reanalysis. Reanalyses are produced using a single version of a data assimilation system coupled with a forecast model constrained to follow observations over a long period. They provide multivariate outputs that are physically consistent, also for variables that are not directly observed (Gelaro et al., 2017). ERA5 is the state-of-the-art reanalysis at the time of writing and was shown to outperform other reanalyses for predicting precipitation using a simpler statistical downscaling method (Horton, 2021). ERA5 provides data with high temporal (hourly) and spatial (0.25°) resolutions.

The weather variables used as input to the DL model should be robust, i.e., not depend too much on the climate model or the NWP model, for the DL model to be transferable to other contexts (Adewoyin et al., 2021). We thus selected frequently-used variables: geopotential height (Z), air temperature (T), relative humidity (RH), total column water (TCW), and both wind components (U, V). All variables were selected at six pressure levels, i.e., 300, 500, 700, 850, 925, and 1000 hPa, except the total column water, which has a single vertical dimension. To reduce the computational costs of training all the networks (see Section 3.2), the spatial resolution of ERA5 data was degraded to 1°. Additionally, the variables were temporally aggregated at a daily time step. The domain on which these variables are used is: latitude = [30, 75] and longitude = [-25, 30].

The precipitation data were also extracted from ERA5 over the same domain and spatial resolution (1°) and aggregated to a daily time step. Our study period is from 1979 to 2021. In this work, heavy precipitation events are identified based on the 95th percentile of the total distribution (1979-2021) for each grid cell (i.e., pixel-wise definition). Similarly, extreme precipitation events are defined as those days exceeding the 99th percentile (Figure S1).

3.2 Methods

3.2.1 Deep Convolutional Neural Networks: selected architectures

CNNs have proven successful in different applications in climate science, including extreme weather forecasting (Racah et al., 2016; Liu et al., 2016), clustered weather patterns prediction (Chattopadhyay et al., 2020), precipitation nowcasting (Shi et al., 2015, 2017), or extreme precipitation (Davenport & Diffenbaugh, 2021; Shi, 2020). They are a type of neural network designed to process high-dimensional data, such as images or geospatial data (LeCun & Bengio, 1995). They have become tremendously popular due to their ability to automatically learn spatial hierarchies of features, from low to high-level patterns (Goodfellow et al., 2016). The principle of CNN relies on a mathematical operation called *convolution*, a specialized linear operation used for feature extraction (Goodfellow et al., 2016). CNNs usually consist of three types of layers: i) convolutional layers that perform the convolution operation, ii) pooling layers that reduce the dimensionality of the inputs, and iii) fully connected layers. The first two types of layers extract and condense the feature information used by dense layers. A typical CNN architecture is often composed of successive convolutional and pooling layers.

Building on CNNs, the popular U-Net, which was originally introduced by Ronneberger et al. (2015) for biomedical image segmentation, has shown good performance in climate applications, such as post-processing weather forecasts (Grönquist et al., 2021; Hess & Boers, 2022), downscaling (e.g., Adewoyin et al., 2021) and precipitation nowcasting (e.g., Trebing et al., 2021). Larraondo et al. (2019) tested several encoder-decoder configurations and found the best results with U-Net-based architectures to forecast total precipitation using geopotential height as input. In Weyn et al. (2020), the authors used a U-Net architecture and mapped the input grid values to a cubed-sphere achieving a good performance to forecast complex surface temperature patterns from a few input atmospheric state variables. The U-Net architecture consists of two parts: a contracting path to capture the context (encoder) and a symmetric expanding path that enables precise localization (decoder). The encoder part is composed of stacked convolutions and pooling operations to extract the features, while the decoder part combines these features (through skip connections) with the upscaled output to reconstruct the spatial information. The encoder-decoder network enables propagating high-resolution features from the contracting path that are combined with the upscaled output (Ronneberger et al., 2015).

Among the DL models presented in the literature for predicting precipitation, we have selected a number of representative studies closely related to our objectives. Given that our approach and model domain differ from the selected original studies, we have adapted the original architectures to our purpose in each case. Table 1 summarizes the inputs originally used in the selected studies. Below, we briefly describe the models considered in our study:

- **Dav-orig**: The original CNN model presented in Davenport and Diffenbaugh (2021) includes two convolutional layers with 16 3x3 filters, followed by two 2x2 max-pooling with a stride of 2. In the original configuration, a dense 16-neuron layer follows the convolution and max-pooling layers, followed by a final classification layer providing the probability of the outcomes. To predict a spatial precipitation field over the European domain, we added a decoder part made of a dense layer, two deconvolution layers, and a final convolution layer, symmetrically to the original model. The model has 48,697 trainable parameters.
- **Dav-64**: We tested a different architecture based on Dav-orig with a latent space of dimension 64 instead of 16. It has 175,081 trainable parameters.
- **Pan-orig**: The CNN model used in Pan et al. (2019) consisted of two convolutional and pooling layers followed by two consecutive dense layers. As in the previous model configurations, a symmetrical decoder part was added to keep the spatial dimensions. The model has 233,014 trainable parameters.
- **CNN-2l**: Following the architectures described above, we additionally tested a convolutional encoder-decoder made of two layers, with a latent space of dimension 64. Further experiments with additional layers were conducted but were not successful. Therefore, the results presented only refer to the CNN-2l. The model has 740,297 trainable parameters.
- **U-Net**: With the success shown by the U-Net in diverse applications, we explored the performance of the original U-Net model with the same structure as proposed by Ronneberger et al. (2015). It has 31,059,073 trainable parameters.
- **Shi-RaNet**: Following the original RaNet architecture proposed in Shi (2020), this model consists of three 3-dimensional CNN layers (using three-dimensional filters) and four fully connected layers, followed by a symmetric decoder part of upscaling layers that allow reconstructing the output into its original size. The model has 1,859,627 trainable parameters.

Table 1. Meteorological variables used by the selected studies. The variables are: sea-level pressure (SLP), geopotential height (Z), air temperature (T), specific humidity (SH), relative humidity (RH), the zonal and meridional wind components (U/V), the total column water vapor (TCW) or precipitable water (PW). The column 'Nb' contains the number of variables used. The table values for Z, T, SH, RH, and U/V represent the pressure levels selected (hPa).

Study	Nb	SLP	Z	T	SH	RH	U/V	TCW/PW
Davenport and Diffenbaugh (2021)	2	1x	500	–	–	–	–	–
Huang (2022)	2	1x	500	–	–	–	–	–
Pan et al. (2019)	4	–	500, 850, 1000	–	–	–	–	1x
Shi (2020)	30	–	300, 500, 700, 850, 925, 1000	300, 500, 700, 850, 925, 1000	–	300, 500, 700, 850, 925, 1000	300, 500, 700, 850, 925, 1000	–

3.2.2 Models implementation

While our primary goal is to assess the model performance to reproduce precipitation extremes, we also tested the models to predict precipitation amounts. Therefore, the implemented models were assessed for different objectives: i) for the prediction of the precipitation amount, ii) for the occurrence of heavy precipitation (i.e., $>$ 95th percentile), and iii) for the occurrence of extremes ($>$ 99th percentile). The model configuration is the same in all cases, the only difference being the activation function of the last layer. A rectified linear unit (ReLU) that ensures non-negative output values is used for predicting the precipitation amount and a sigmoid is applied for predicting the probability of heavy/extreme events. It is important to note that all models were trained independently. The loss function used was the mean squared error (MSE) for the prediction of the precipitation amount and the weighted binary cross-entropy for the prediction of the occurrence of extremes (with weights computed to balance both classes). These scores were computed pixel-wise and aggregated over the domain. An early-stopping strategy has been used, with a maximum of 200 epochs. For all models, dropout and spatial dropout for the convolutional layers have been used.

A class was written in Python to generate the different model architectures with multiple options and handle common tasks, such as an eventual initial zero-padding when necessary, and output cropping. It also sets the final activation layer to ReLU for the prediction of precipitation values or sigmoid for the prediction of the probability of extremes. The models were implemented using Keras (Chollet et al., 2015) and designed according to the description in the related paper.

The input data is a tensor of shape 46x56x31; 31 represents the number of atmospheric fields (i.e., channels): six fields for Z, RH, T, U, V, and one for TCW; 46x56 represents the spatial dimensions (latitude x longitude) of the domain considered. All models use the same number of channels (i.e., 31), except the Shi-RaNet model, for which TWC was excluded as 3D variables are required. The training period ranges from 1979 to 2005 and validation from 2005 to 2015. The testing period covers from 2016 to 2021.

3.2.3 Baseline model

To compare the performance of the DL models with more traditional methods, a random forest (RF) model (Breiman, 2001) was used as baseline. The RF was fed with the same input data and trained/tested on the same periods as the DL architectures. As RF models do not predict spatial fields by nature, one model was here trained per pixel of the domain and then used to predict for that same pixel. Then, all predicted pixel-wise time series were aggregated into maps to provide daily fields.

As with the DL models, two different kinds of contexts were considered: the prediction of i) the precipitation amount using a regressor RF and ii) the occurrence of heavy/extreme events (95/99th percentile) using a classifier. In the later case, the weights between event occurrence and non-occurrence were also balanced. Different values of the maximum depth of RFs, which is an important parameter to avoid overfitting, have been tested and the optimal one (4) was further used.

3.2.4 Feature importance: Layer-wise Relevance propagation

We used layer-wise relevance propagation (LRP), an explanation technique applicable to ML models (e.g. Montavon et al., 2018), to better understand the importance of the input variables for heavy precipitation events, i.e., which variables are more important for the network to make a prediction. Among the existing methods of DL interpretation, LRP is a backward propagation technique used for explaining complex network outputs. The LRP creates heatmaps, which in our case help identify the most relevant regions of the input for predicting a heavy precipitation event (Barnes et al., 2022). Similarly to recent studies that used LRP in geoscience applications (e.g. Davenport & Diffenbaugh, 2021; Toms et al., 2020), we apply the α-β rule with $\alpha = 1$ and $\beta = 0$ to identify locations for which higher activation values positively contribute to a likely output (i.e. predicted class). Thus, with this formulation, only positive contributions to the neural network output are tracked. It is therefore well suited to categorical output (i.e., extreme or not extreme). We additionally tested other methods, such as the gradient and the deep Taylor, but for simplicity and easier output interpretation, we only considered the alpha-beta rule, specifically the $\alpha_0\beta_1$.

The LRP produces a map with the same dimensions as the input, where the pixel values indicate the importance of the predicted class. A total of 31 maps (i.e., 31 input variables) are obtained for each day. Then, we computed composite maps (for each input feature separately) by calculating for every pixel the average value of the relevance of a specific input feature for all days with an extreme event at that same pixel, within the training period: $\overline{R} = \frac{1}{N_i}\sum R$. For comparison, we considered a larger area of influence for each pixel by calculating the averages of the maximum relevance within a small spatial domain for each feature when an event occurred:

$$\overline{R} = \frac{1}{N_i}\sum max(R \mp z);$$

where z represents the number of the closest pixels to calculate the relevances at each grid cell. We performed additional sensitivity analyses for different values of z and decided to use $z = 3$ as a good compromise to account for local processes that might be relevant for pixel-wise precipitation events. It is important to note that the averages of the relevances were calculated for the *true* extremes.

As detailed below (see Section 4.3), after selecting our best model for predicting precipitation, we apply the LRP to examine the most important features for simulating heavy precipitation events. Based on the relevance values obtained for the training sample, we ranked the predictors by their average relevance. These values were obtained by averaging the composite maps produced for each input feature. Then, we conducted a number of experiments for differing subsets of predictors to examine the role of the number of features in the model performance.

4 Results

4.1 Networks performance

We noticed that the loss values greatly vary when comparing the architectures. Overall, the loss decreases relatively consistently for the different models. The U-Net shows the lowest values, and its optimization stops significantly earlier than other models (Figures S2, S3).

We trained the models separately predicting precipitation amounts (e.g. as a regression task) and precipitation events (e.g. as a classification task). In the first case, we assessed the prediction of the precipitation amount through the RMSE, and we further estimated the predicted threshold exceedances (95th and 99th percentile for each pixel) to compute the precision and recall scores (Table 2 for the 95th percentile and Table 3 for the 99th percentile). The U-Net outperformed the rest of the models for predicting precipitation amounts and provided the lower RSME and the highest precision and recall scores when assessing the threshold exceedances.

Table 2. Scores of the tested models when trained to **predict the precipitation amount**. Precision and recall are computed for the exceedance of the **95th percentile**. The best scores are highlighted in bold.

Model id	RMSE train	RMSE test	Precision train	Precision test	Recall train	Recall test
Random forest	2.67	2.93	0.73	0.66	0.27	0.23
Dav-orig	3.19	3.33	0.55	0.51	0.21	0.20
Dav-64	2.74	2.93	0.65	0.62	0.37	0.34
Pan-orig	2.42	2.58	0.68	0.66	0.47	0.44
CNN-2l	2.35	2.68	0.69	0.63	0.50	0.43
U-Net	**1.43**	**1.73**	**0.81**	**0.78**	**0.69**	**0.64**
Shi-RaNet	3.21	3.43	0.60	0.53	0.18	0.15

Table 3. Scores of the tested models when trained to **predict the precipitation amount**. Precision and recall are computed for the exceedance of the **99th percentile**. The best scores are highlighted in bold.

Model id	**RMSE train**	**RMSE test**	**Precision train**	**Precision test**	**Recall train**	**Recall test**
Random forest	2.66	2.93	0.67	0.28	0.09	0.05
Dav-orig	3.21	3.35	0.31	0.13	0.02	0.02
Dav-64	2.73	2.91	0.58	0.46	0.16	0.12
Pan-orig	2.44	2.59	0.68	0.63	0.26	0.22
CNN-2l	2.36	2.67	0.68	0.57	0.31	0.21
U-Net	**1.46**	**1.73**	**0.84**	**0.79**	**0.52**	**0.43**
Shi-RaNet	3.01	3.30	0.57	0.31	0.07	0.03

The forecast skills of heavy and extreme precipitation events were evaluated in terms of the AUC (ROC under curve area), the precision and recall scores based on a probability threshold of 0.5 Tables 4 and 5 show the score values obtained for classifying both heavy (>95th) and extreme (>99th) precipitation events.

Similarly to the regression case, the results show clearly that U-Net, which has significantly more trainable parameters, is the best to predict precipitation extremes. However, a difference between both settings becomes obvious: when trained for the prediction of extremes, the model's outputs result in a much higher recall than when trained for the precipitation amount while presenting a lower precision. The models trained for the extremes predict them better than when trained for the whole precipitation distribution (i.e., Table 3), but overestimate the number of extreme events (i.e., Table 5). It can be expected that balancing the weights differently in the weighted binary cross-entropy will result in other recall and precision scores.

Table 4. Scores of the tested models when trained to **predict precipitation extremes**. Precision and recall are computed for the exceedance of the **95th percentile**. The best scores are highlighted in bold.

Model id	AUC train	AUC test	Precision train	Precision test	Recall train	Recall test
Random forest	0.90	0.86	0.27	0.27	0.93	0.85
Dav-orig	0.90	0.89	0.17	0.18	0.86	0.83
Dav-64	0.95	0.93	0.25	0.25	0.91	0.87
Pan-orig	0.96	0.95	0.26	0.26	0.95	0.92
CNN-2l	0.97	0.94	0.27	0.26	0.96	0.89
U-Net	**0.99**	**0.98**	**0.38**	**0.38**	**0.99**	**0.95**
Shi-RaNet	0.92	0.88	0.18	0.17	0.91	0.84

Table 5. Scores of the tested models when trained to **predict precipitation extremes**. Precision and recall are computed for the exceedance of the **99th percentile**. The best scores are highlighted in bold.

Model id	AUC train	AUC test	Precision train	Precision test	Recall train	Recall test
Random forest	0.90	0.89	0.05	0.06	0.98	0.95
Dav-orig	0.94	0.92	0.05	0.05	0.93	0.89
Dav-64	0.98	0.96	0.10	0.09	0.96	0.88
Pan-orig	0.98	0.97	0.09	0.09	0.98	0.93
CNN-2l	0.97	0.94	0.07	0.07	0.97	0.89
U-Net	**0.99**	**0.99**	**0.17**	**0.17**	**0.99**	**0.97**
Shi-RaNet	0.93	0.89	0.05	0.05	0.92	0.80

We further analyze the ability of the DL models to represent the spatial distribution of precipitation events realistically. To do so, we examine the predictions of the different models for the day with the highest amount of observed precipitation exceeding the 95th percentile and the 99th percentile during the test period and over the considered domain. As for the scores, we also compare the RF performance to capture the spatial distribution of extreme precipitation events (Figures S5 and S6).

Figures 1 and 2 show the results of the models trained for the prediction of the precipitation amount (two first columns) and the results of the models trained for the prediction of the occurrence of extremes (last column). From Figure 1 it can be seen that, in general, most of the models simulate fairly well heavy precipitation events. In particular, Dav-64, Pan-orig and CNN-2l show consistent patterns when compared with the truth (i.e., ERA5). The differences between the models become larger when comparing their performance in capturing extreme precipitation events (Figure 2). While the overall scores obtained for the baseline RF model show a close performance to some of the DL architectures (e.g., Dav-orig, CNN-2l), the RF represent poorly the spatial distribution of the selected precipitation event, compared to the DL models (Figure S5 and S6). This highlights the ability of CNN to extract the spatial information, being more efficient to treat complex spatial features. In that case, it can be observed that U-Net is superior and reproduces the closest pattern to the *truth*. In agreement with the skill scores in Tables 2-5, the U-Net outperforms the rest of the models for both the amount of precipitation and the threshold exceedances. Although U-Net simulates relatively well the precipitation fields, as mentioned before, the model tends to predict a high number of false positives, as shown by a lower precision skill (compared to the recall skill).

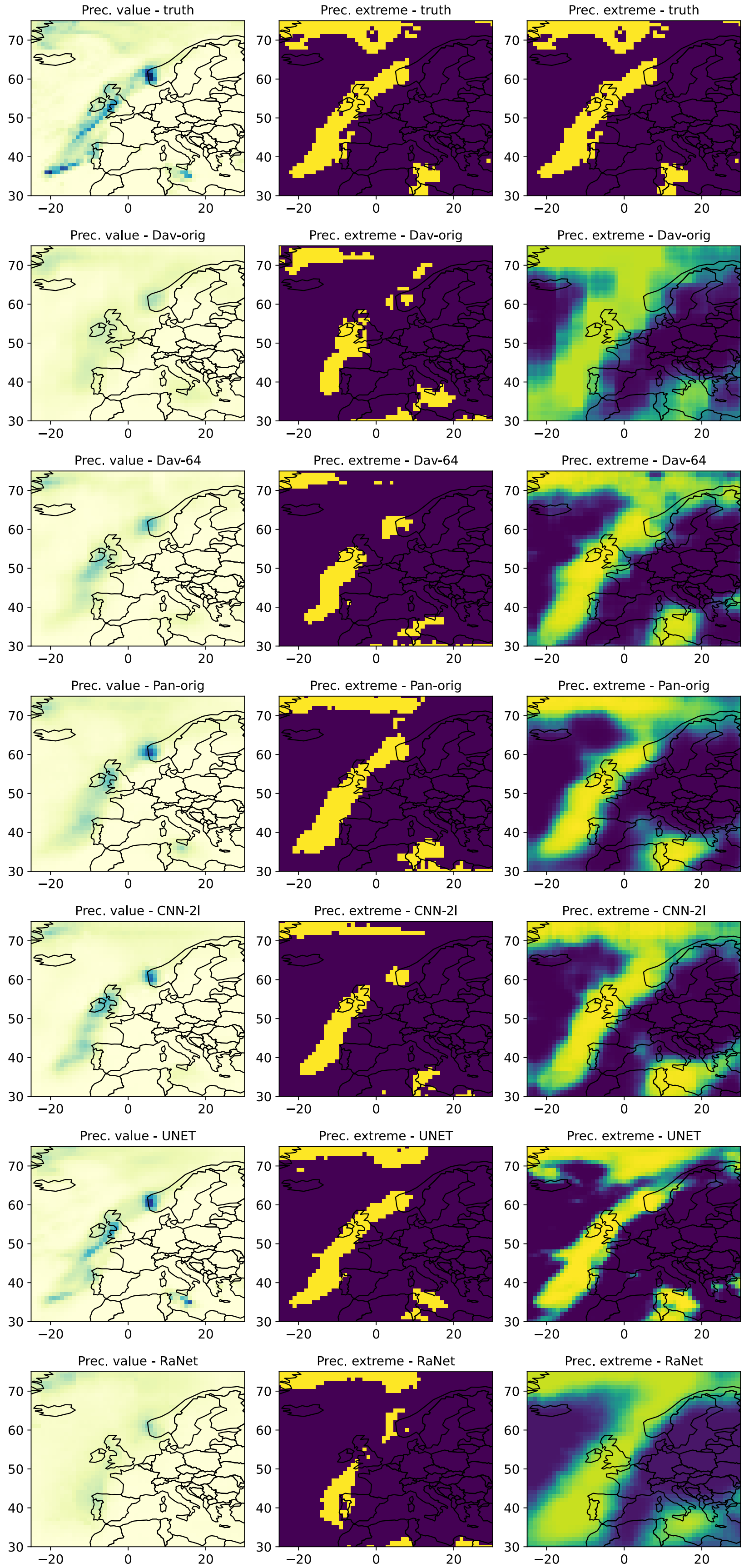

Figure 1. First row: true values of the precipitation amount and the corresponding threshold exceedance for the **95th percentile**. Next rows: the prediction of each model for the same date, in terms of precipitation amount (first column), the corresponding threshold exceedance (second column), and the probability of the occurrence of heavy precipitation (third column).

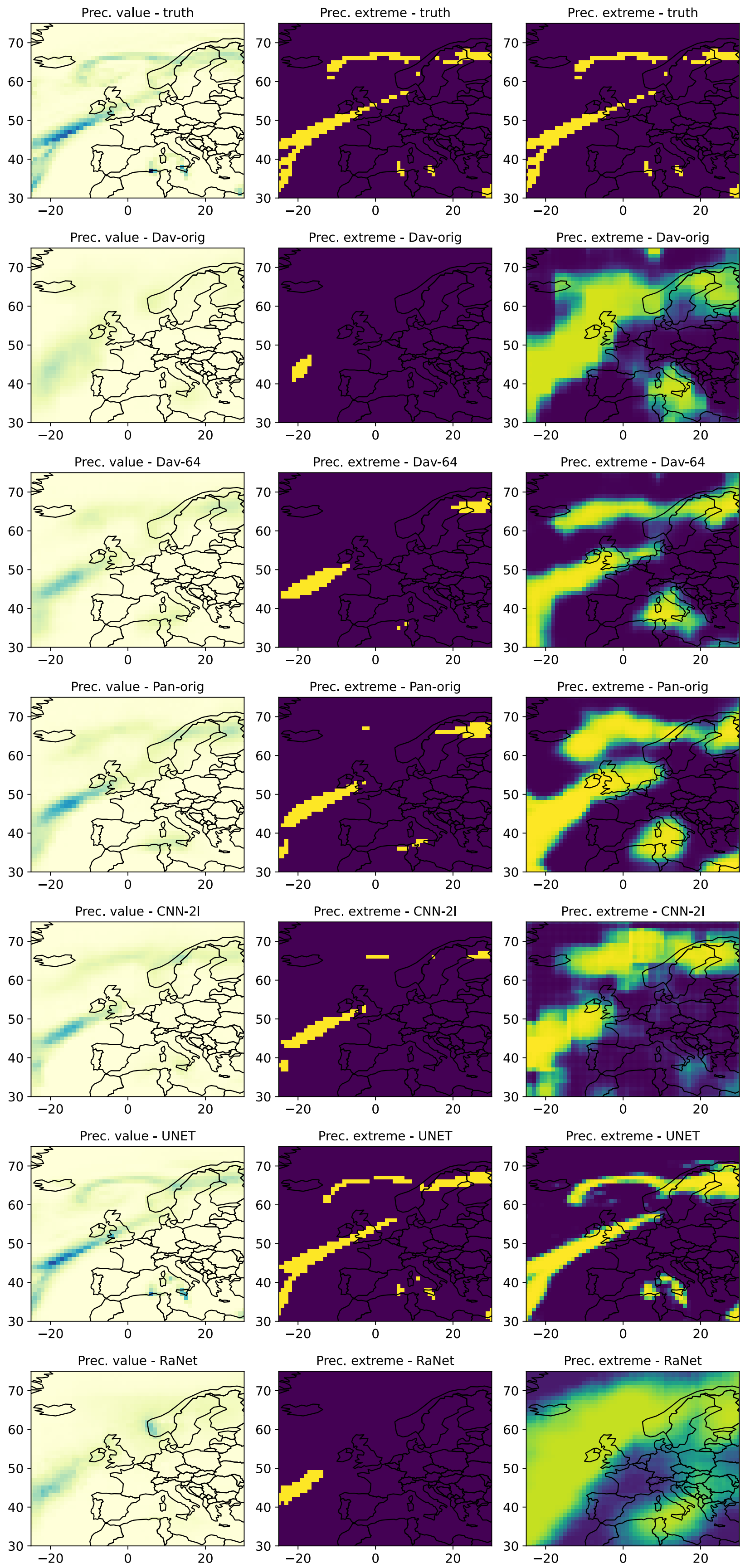

Figure 2. First row: true values of the precipitation amount and the corresponding threshold exceedance for the **99th percentile**. Next rows: the prediction of each model for the same date, in terms of precipitation amount (first column), the corresponding threshold exceedance (second column), and the probability of the occurrence of extreme precipitation (third column).

4.2 Assessment of U-Net variants

Motivated by the good performance of U-Net in simulating precipitation events, we conducted further experiments to assess the predictive capabilities of several U-Net-based architectures only for precipitation events.

4.2.1 U-Net with attention

Recently, within the attention framework, Trebing et al. (2021) proposed an adapted U-Net with a combination of attention modules and depthwise-separable convolutions for precipitation nowcasting. Introducing an attention mechanism into the convolutional neural network structure has also become popular in image segmentation processes (Oktay et al., 2018). In particular, the Attention U-Net proposed by Oktay et al. (2018) exploits the use of Attention Gates added to the encoder-decoder structure. This soft-attention mechanism is implemented for the skip connections. The Attention Gates actively suppresses activations in irrelevant regions and, thus, reduces the number of redundant features. The authors showed that the use of Attention Gates improved the prediction performance of U-Net as the model learned to focus on useful features information, enhancing the accuracy of the network in locating tissues and organs, in the medical context. Based on this, we also tested whether the inclusion of Attention Gates improve the accuracy of simulating extreme precipitation events. While using an attention gate in U-Net showed an improvement for medical image datasets (Oktay et al., 2018), this was not the case in our application, as the results showed similar performances with or without the attention gates (Table 6). Therefore, the attention gates were not further used in the following analyses.

Table 6. Scores of the original U-Net and the U-Net with attention when trained to predict heavy precipitation. Precision and recall are computed for the exceedance of the 95th percentile.

Model id	**AUC train**	**AUC test**	**Precision train**	**Precision test**	**Recall train**	**Recall test**
U-Net	0.987	0.980	0.384	0.387	0.979	0.950
U-Net Attention	0.986	0.981	0.378	0.382	0.983	0.953

4.2.2 Sensitivity to U-Net depth and number of features

As the U-Net hyperparameters, such as the network depth or the number of feature maps, greatly affect the number of trainable weights and the model performance, we explored the effect of the U-Net architecture design on the prediction of precipitation events, in particular, heavy precipitation events. Thus, we conducted several sensitivity analyses to explore whether reducing the number of hyperparameters would lead to comparable results to the original U-Net. Specifically, we focused on the architecture size, i.e., the depth of the network that we measured in terms of the number of *encoder-decoder* levels. Starting from the original network made of 4 levels (Ronneberger et al., 2015), we decreased the number of levels (i.e., network depth) iteratively until the simplest network (i.e., 1 level).

In addition, for each U-Net-based network, we further assessed the importance of the predictors in the model performance. With the feature selection, we aim to assess whether reducing the number of features, which would also reduce the computational effort, results in a similar or better performance than the full set of features (i.e., 31). A typical forward/backward stepwise selection procedure where the predictors are included/removed one at a time would be computationally expensive. Thus, the predictors were included in the models five at a time according to the ranking provided by the LRP (see Fig. 3). For example, the first subset consists of the top five predictors (RH700, V1000, RH850, RH500, and U1000), the second subset includes the top ten predictors, and so on.

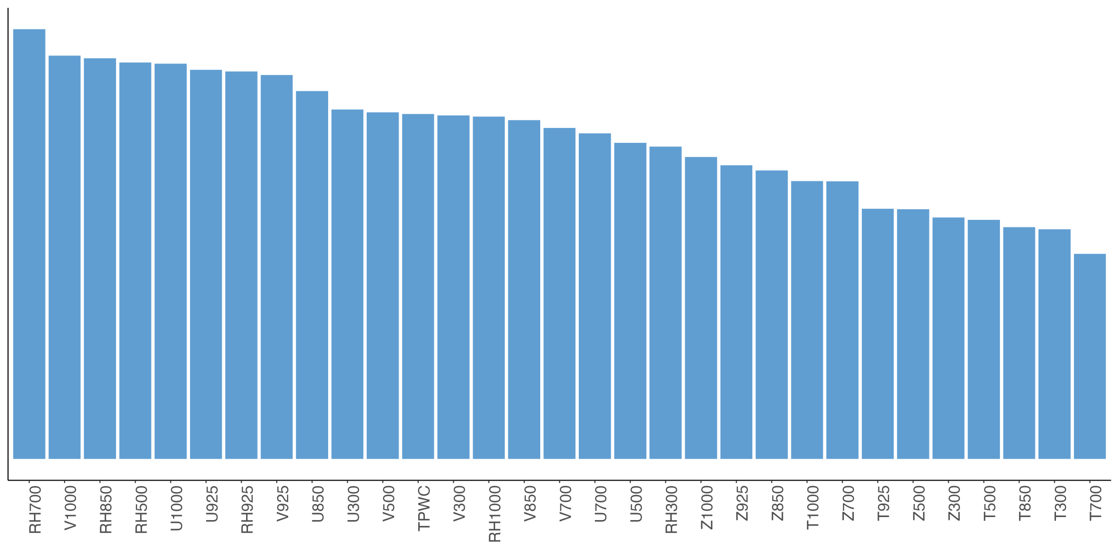

Figure 3. Ranked relevances (averages) obtained for heavy precipitation events in the training sample (1979-2005) for each feature.

By jointly varying the architecture depth and the number of inputs, we assessed four U-Net architectures, each one trained separately for 6 predictor subsets, resulting in a total of 30 models (four levels and six predictor subsets). It is important to note that all models were trained separately. As the size of the architecture is reduced, the number of trainable parameters considerably decreases (Fig. 4).

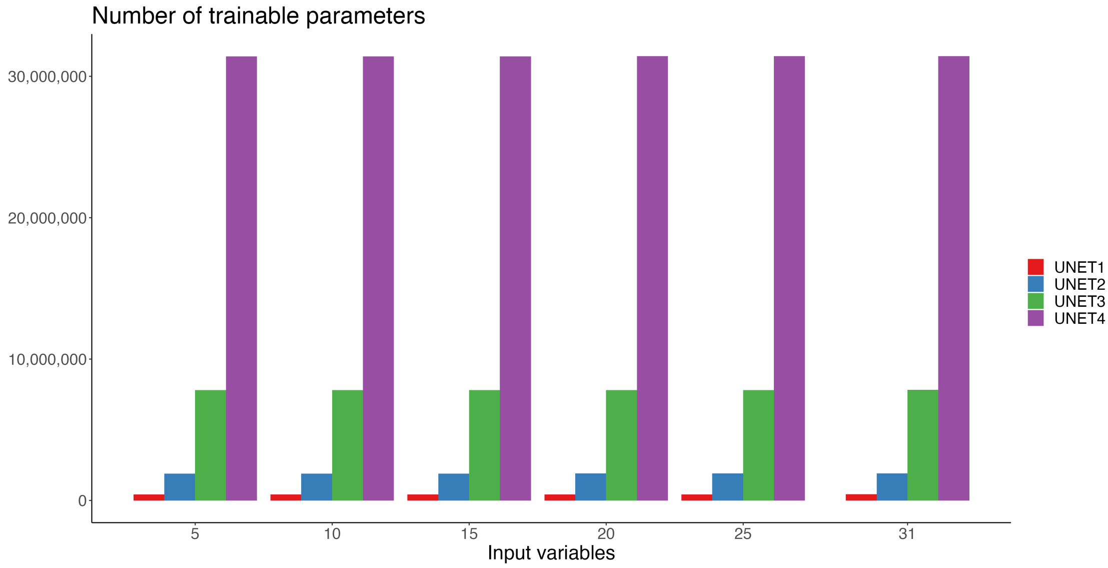

Figure 4. Number of trainable parameters for the different architecture sizes for the different subsets of predictors. Note that the number of trainable parameters changes with the number of input data even though the changes are small.

As stated in the previous Section, we evaluate the forecast skill of heavy precipitation events through the categorical skill scores commonly used for classification problems and can be obtained from the contingency table. The AUC, precision, and recall scores were calculated for both training and test datasets. Figure 5 illustrates the results corresponding to the U-Net architectures used in the experiments for different subsets of predictors.

It can be observed that the performance is considerably lower for the input of 5 features and improves when increasing the number of predictors to 10 or 15. Overall, the proportion of heavy precipitation events that are correctly classified (i.e., precision) is higher when increasing the number of features for the deeper U-Nets (e.g., UNET3, UNET4). However, such skill improvement with the number of features is not observed for the shallowest U-Nets (UNET1, UNET2) and the models show the highest precision when using 15 and 20 features. It should be noted that these optimums likely depend on the random seed and some variability is expected between different random seeds. These results show anyway that more data does not always means better performance. The recall values tend to increase with the number of predictors, but only up to 10 or 15 features.

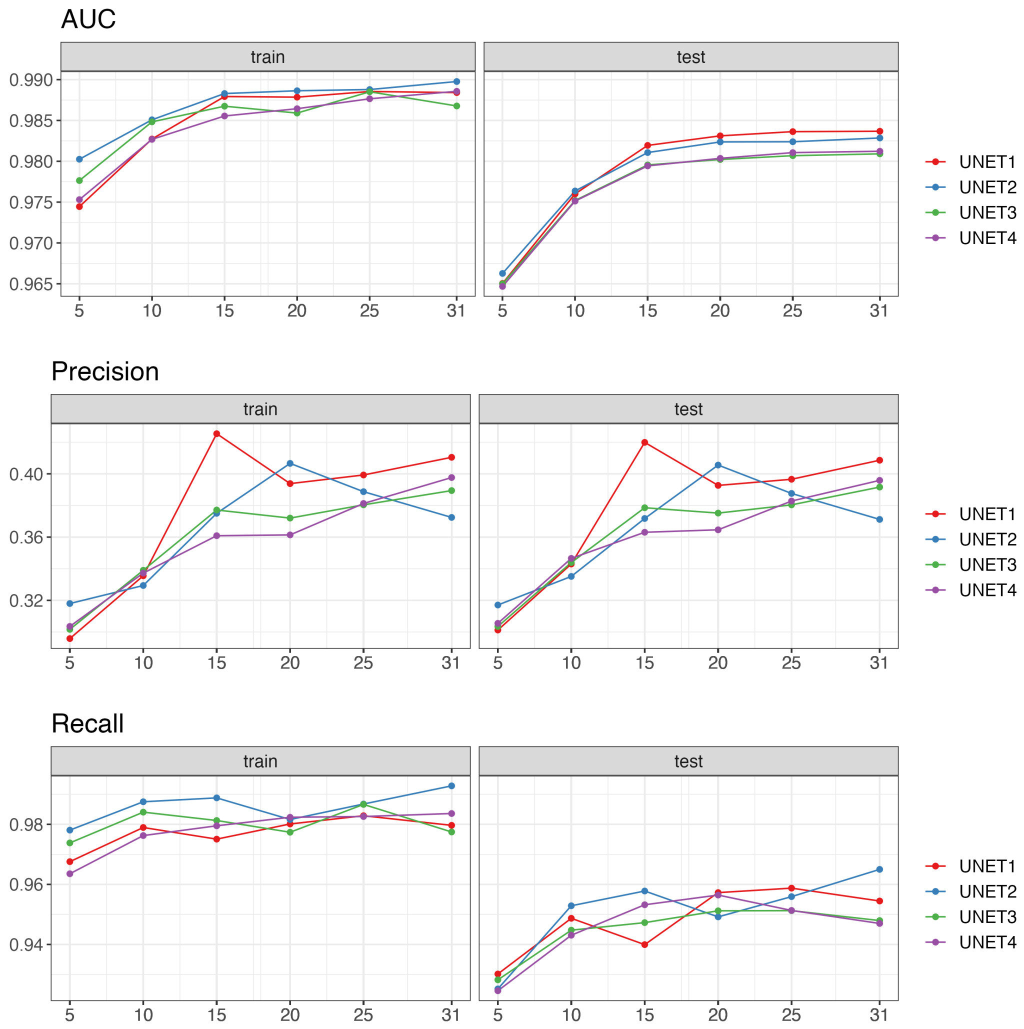

Figure 5. Scores obtained for the U-Net-based networks: U-Net1 (1 levels), U-Net2 (2 levels), U-Net3 (3 levels) and U-Net4 (4 levels) for different subsets of predictors according to the LRP-ranking.

4.3 Interpretability: LRP

The LRP previously used was also mapped to visualize which features and which geographical region are important for the U-Net network to predict a heavy precipitation event. We first examined the composite LRP maps (Sect. 3.2.4) for all heavy events occurring during the training period (1979-2005). These maps highlight the relevant features at a pixel scale for predicting heavy precipitation at that same pixel (Fig. 6). Note that we apply the α-β rule, which only considers positive activations. From Figure 6 it can be observed that some features are more relevant inland (e.g., relative humidity fields) while others have an increased relevance for events occurring over the sea (e.g., geopotential height). Overall, the relative humidity shows the highest values, followed by both wind components, particularly in western and southern Europe. The high relevance of the wind components in some areas reflects the dependence between extreme precipitation events and strong wind conditions due to the same mesoscale and/or synoptic features, as shown by previous studies (Martius et al., 2016). For example, one can observe the higher relevance values of the zonal (e.g., U850, U925) and meridional wind (e.g., V925) in the Iberian Peninsula, which often experiences concurrent extreme precipitation and winds conditions, mostly related to extra-tropical cyclones and their atmospheric fronts (Hénin et al., 2021). We can also distinguish the relevance of the meridional wind (e.g., V500) for the alpine region, which is known to be related to heavy precipitation events due to the orographic forcing of air masses that transport moisture from the Mediterranean. This influence of the atmospheric circulation comes in pair with the moisture information, heavily represented by the relative humidity variable at 700 hPa (RH700).

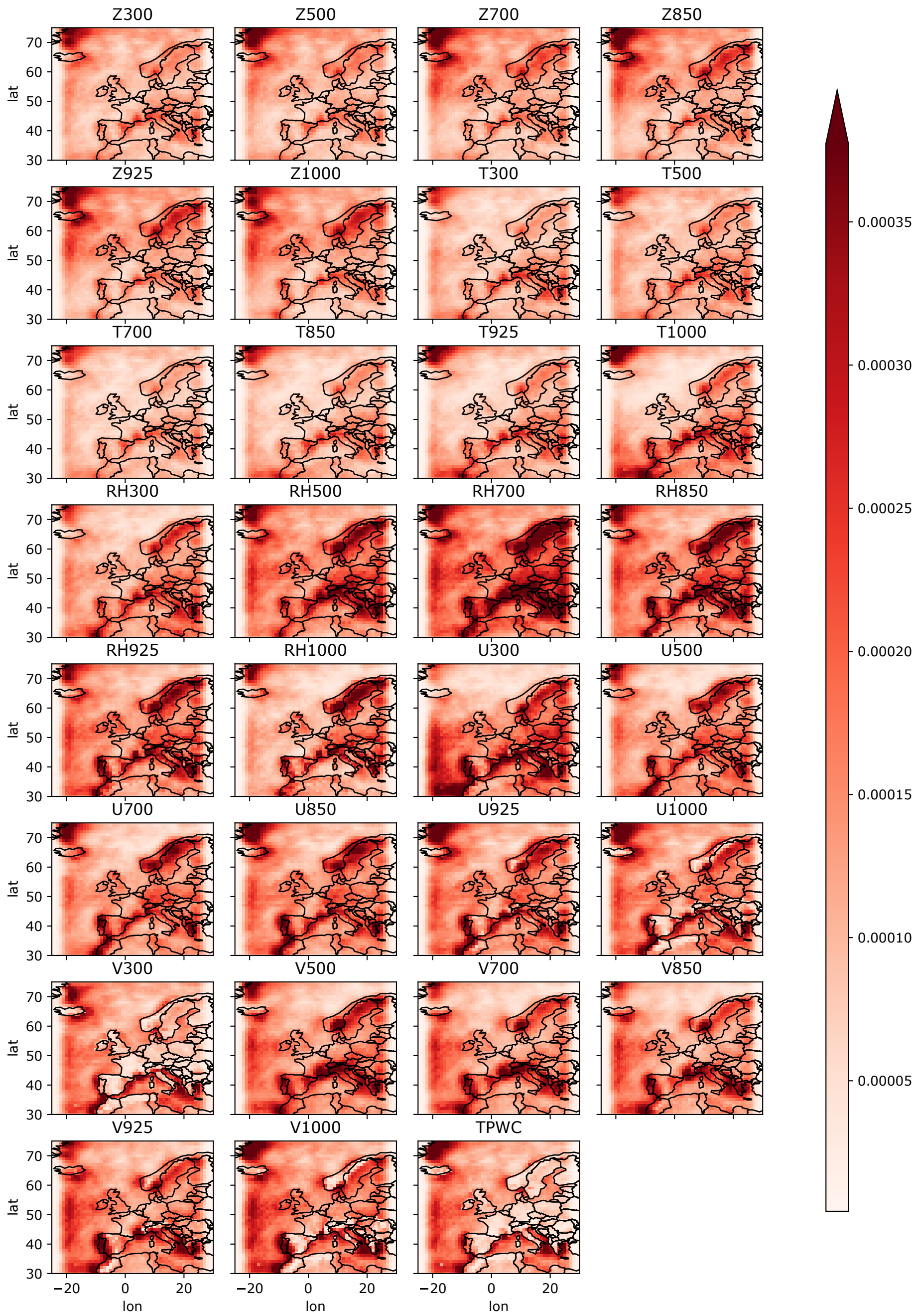

Figure 6. Composite relevance maps for heavy precipitation events ($> 95th$ percentile) derived from the U-Net original architecture during the training period (1979-2005) for each feature.

We then examined the relevance of predictors for single extreme precipitation events, starting by analyzing the same event that led to the highest amount of observed precipitation exceeding the 95th percentile (Figure 1). The meteorological context during that day, 13th October 2018, was characterized by an extra-tropical cyclone called Leslie, which was a large long-lived tropical cyclone in the Atlantic that became a powerful post-tropical system and made land in Portugal on 13th October (Mandement & Caumont, 2021). This remarkable event resulted in heavy precipitation in several regions in Western Europe (e.g., Portugal, France). Also that day, another storm called Callum that began as an Atlantic depression led to strong winds and flooding over the U.K.

After calculating the LRP for the days during that particular episode (13-15 October 2018) for each feature, we averaged them over all input variables. Figure 7 illustrates the temporal evolution of the influence of the inputs for the precipitation event. The maps show the regions that are physically related to precipitation extremes. For example, on the 13th October the networks focus on the U.K., as the region of influence, although late the same day, another storm reached the western coast of Portugal. It must be noted that we use daily averages, therefore, it seems reasonable for the model to look at the regions where the inputs have major weights. It can be observed how the region of influence shifts south-eastwards, which is physically consistent with the development of the synoptic situation associated with that heavy precipitation episode (Mandement & Caumont, 2021).

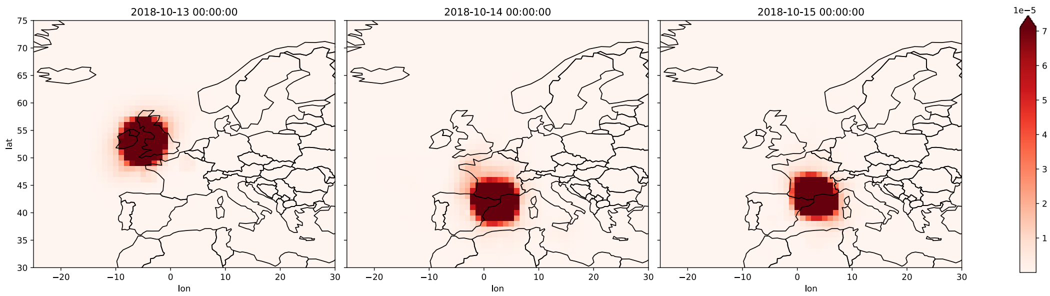

Figure 7. Temporal evolution of the averaged relevance over all input variables during the episode of October 2018.

In addition, we analyzed another episode of heavy precipitation that occurred in summer 2021, specifically during the period 13th to 15th July 2021, which led to severe flooding, particularly in North Rhineland-Palatinate in Germany, part of Belgium, and the Netherlands (Kreienkamp, 2022). While the U-Net is able to capture this episode, a larger spatial extension was predicted, indicating that the model overestimates the geographical area affected by the event (e.g., see Figure S3). This is expected due to a higher number of *False positive*, as shown by the precision skill score (see Table 3).

Similar to the episode of October 2018, the model tends to look at the geographical region where heavy rainfall occurred (e.g., western and central Europe, see Figure S4). The LRP maps for this event show similar patterns for all the input features with a common area of higher relevance in the Netherlands, Belgium, northwest of France, and west of Germany. As shown in Fig. 7, the network finds the most relevant geographical regions at the same location as the heavy precipitation event evolves. This indicates that the local predictors contain enough information to predict the event and that no remote information is needed. The LRP maps focus on the regions physically related to the episode, and no relevant areas are found outside central and west of Europe.

5 Conclusions

The use of machine learning has exponentially grown in the past years in a wide number of fields. In particular, deep learning methods have shown enormous potential to address complex Earth Science problems, which might be useful to tackle climate change-related issues. Here, we have presented an intercomparison of existing architectures used to predict precipitation, either for aggregated precipitation (i.e., over an extended region) or spatial precipitation fields. A total of six models consisting of different CNN configurations were tested. We examined the forecast skill not only to simulate heavy and extreme precipitation events but also to predict the amount of precipitation over the European domain. For the interpretability of the networks, we applied a layer-wise propagation technique, which was further used as a tool of feature selection to test the importance of the number of input parameters on the model performance. It is important to note that while some of these DL topologies have been previously presented in the literature, the original application slightly differs from ours, and more importantly, the original configuration was adapted to our purposes (e.g., in each case, we added a decoder part to preserve the spatial dimensions of the input data).

In general, most of the analyzed DL were able to reproduce reasonably well the occurrence of precipitation events. However, we found that the U-Net outperformed the rest of the tested architectures by a large margin, which is in line with previous studies (Hess & Boers, 2022; Larraondo et al., 2019) that used a U-Net architecture to simulate precipitation. In general, the skill scores that measure the precision to classify heavy precipitation events (i.e., >95th percentile) were higher than those obtained for extreme precipitation events (i.e., >99th percentile), due to the unbalanced number of classes where the number of extremes is significantly reduced in the training data.

Motivated by the good performance shown by the U-Net architecture, we additionally conducted a number of experiments on U-Net-based configurations to examine how the network depth and the number of inputs play a role in the performance of the model. As expected, the network showed the poorest performance when using only a few input variables for all the U-Net-based networks (i.e., different levels of depth). Overall, a deeper network achieves slightly better results with the largest number of inputs, especially regarding the precision scores. On the contrary, shallower networks seem to achieve similar skill scores for a lower number of input data. We noticed that from 15 features on, the models only gained a modest improvement overall, suggesting that a smaller number of input would lead to similar results with less computational effort.

While the original U-Net already showed a good performance, we found that a shallower network, in terms of number levels compared to the original architecture, would be sufficient to classify heavy precipitation events correctly. This likely means that, for this spatial resolution and with no temporal extrapolation, most of the information needed to forecast precipitation is available at the location where the precipitation occurs. Our results showed that in such a context, a shallower U-Net, which significantly reduces the number of trainable parameters and the computationally time, is able to predict fairly well precipitation events.

6 Data Availability Statement

The ERA5 data is available for download at the Copernicus Climate Change Service (C3S; Hersbach et al., 2020; https://cds.climate.copernicus.eu/cdsapp#!/dataset/reanalysis-era5-pressure-levels). The code used for the analysis is available in:
`https://github.com/ML-precip/precip-predict`

References

Adewoyin, R. A., Dueben, P., Watson, P., He, Y., & Dutta, R. (2021). TRU-NET: a deep learning approach to high resolution prediction of rainfall. *Machine Learning*, *110*(8), 2035–2062. doi: 10.1007/s10994-021-06022-6

Ayzel, G., Heistermann, M., Sorokin, A., Nikitin, O., & Lukyanova, O. (2019). All convolutional neural networks for radar-based precipitation nowcasting. *Procedia Computer Science*, *150*, 186-192. doi: 10.1016/j.procs.2019.02.036

Barnes, E. A., Barnes, R. J., Martin, Z. K., & Rader, J. K. (2022). This looks like that there: Interpretable neural networks for image tasks when location matters. *Earth and Space Science Open Archive*, 34. doi: 10.1002/essoar.10509984.2

Bauer, P., Thorpe, A., & Bruner, G. (2015). The quiet revolution of numerical weather prediction. *Nature*, *525*, 47-55. doi: 10.1038/nature14956

Breiman, L. (2001). Random forests. *Machine Learning*, *45*, 5-32. doi: https://doi.org/10.1023/A:1010933404324

Chattopadhyay, A., Hassanzadeh, P., & Pasha, S. (2020). Predicting clustered weather patterns: A test case for applications of convolutional neural networks to spatio-temporal climate data. *Sci Rep*, *10*, 1317. doi: 10.1038/s41598-020-57897-9

Chollet, F. (2017). Xception: Deep learning with depthwise separable convolutions. In *2017 ieee conference on computer vision and pattern recognition (cvpr)* (p. 1800-1807). doi: 10.1109/CVPR.2017.195

Chollet, F., et al. (2015). *Keras.* `https://github.com/fchollet/keras`. GitHub.

Civitarese, D. S., Szwarcman, D., Zadrozny, B., & Watson, C. (2021). Extreme Precipitation Seasonal Forecast Using a Transformer Neural Network. *arXiv*. Retrieved from `http://arxiv.org/abs/2107.06846`

Davenport, F. V., & Diffenbaugh, N. S. (2021). Using Machine Learning to Analyze Physical Causes of Climate Change: A Case Study of U.S. Midwest Extreme Precipitation. *Geophysical Research Letters*, *48*(15). doi: 10.1029/2021GL093787

Donat, M., Lowry, A., Alexander, L., P., O., Maher, N., & Diffenbaugh, N. S. (2016). More extreme precipitation in the world's dry and wet regions. *Nature Clim Change*, *6*, 508-513. doi: 10.1038/nclimate2941

Gao, X., & A., S. C. (2019). Mid-Western US heavy summer-precipitation in regional and global climate models: the impact on model skill and consensus through an analogue lens. *Clim Dyn*, *6*, 1569–1582. doi: 10.1007/s00382-018-4209-0

Gelaro, R., McCarty, W., Suárez, M. J., Todling, R., Molod, A., Takacs, L., … Zhao, B. (2017). The modern-era retrospective analysis for research and applications, version 2 (MERRA-2). *J. Climate*, *30*(14), 5419–5454. doi: 10.1175/JCLI-D-16-0758.1

Goodfellow, I., Bengio, Y., & Courville, A. (2016). *Deep learning. MIT Press.* Retrieved from `http://www.deeplearningbook.org`

Grönquist, P., Yao, C., Ben-Nun, T., Dryden, N., Dueben, P., Li, S., & Hoefler, T. (2021). Deep learning for post-processing ensemble weather forecasts. *Philosophical Transactions of the Royal Society A: Mathematical, Physical and Engineering Sciences*, *379*(2194), 20200092. doi: 10.1098/rsta.2020.0092

Hersbach, H., Bell, B., Berrisford, P., Hirahara, S., Horányi, A., Muñoz-Sabater, J., … Thépaut, J. N. (2020). The ERA5 global reanalysis. *Quarterly Journal of the Royal Meteorological Society*, *146*(730), 1999–2049. doi: 10.1002/qj.3803

Hess, P., & Boers, N. (2022). Deep learning for improving numerical weather prediction of heavy rainfall. *Journal of Advances in Modeling Earth Systems*, *14*(3), e2021MS002765. doi: 10.1029/2021MS002765

Hill, A. J., & S., S. R. (2022). Forecasting excessive rainfall with random forests and a deterministic convection-allowing model, weather and forecasting. *Weather and Forecasting*, *36*(5), 1693-1711. doi: https://journals.ametsoc.org/view/journals/wefo/36/5/WAF-D-21-0026.1.xml

Hill, G. R., A. J. Herman, & S., S. R. (2022). Forecasting severe weather with random forests. *Monthly Weather Review*, *148*(5), 2135-2161. doi: https://journals.ametsoc.org/view/journals/mwre/148/5/mwr-d-19-0344.1.xml

Horton, P. (2021). Analogue methods and ERA5 : Benefits and pitfalls. *International Journal of Climatology*(November), 1–19. doi: 10.1002/joc.7484

Huang, W. (2022). Extreme precipitation forecasting using attention augmented convolutions. *CoRR*, *abs/2201.13408*. Retrieved from https://arxiv.org/abs/2201.13408

Hwang, J., Orenstein, P., Cohen, J., Pfeiffer, K., & Mackey, L. (2019). Improving subseasonal forecasting in the western U.S. With machine learning. *Proceedings of the ACM SIGKDD International Conference on Knowledge Discovery and Data Mining*, 2325–2335. doi: 10.1145/3292500.3330674

Hénin, R., Ramos, A. M., Pinto, J. G., & Liberato, M. L. R. (2021). A ranking of concurrent precipitation and wind events for the iberian peninsula. *International Journal of Climatology*, *41*(2), 1421-1437. doi: 10.1002/joc.6829

Kreienkamp, e. a., F. (2022). Rapid attribution of heavy rainfall events leading to the severe flooding in Western Europe during July 2021. *World Weather Attribution*. Retrieved from https://www.worldweatherattribution.org/wp-content/uploads/Scientific-report-Western-Europe-floods-2021-attribution.pdf

Larraondo, P. R., Renzullo, L. J., Inza, I., & Lozano, J. A. (2019). A data-driven approach to precipitation parameterizations using convolutional encoder-decoder neural networks. *arXiv*. doi: 10.48550/ARXIV.1903.10274

LeCun, Y., & Bengio, Y. (1995). Convolutional networks for images, speech, and time series, the handbook of brain theory and neural networks. *MIT Press*, 255–258.

Liu, Y., Racah, E., Prabhat, Correa, J., Khosrowshahi, A., Lavers, D., ... Collins, W. (2016). Application of deep convolutional neural networks for detecting extreme weather in climate datasets. *arXiv*.

Mandement, M., & Caumont, O. (2021). A numerical study to investigate the roles of former hurricane leslie, orography and evaporative cooling in the 2018 aude heavy-precipitation event. *Weather Clim. Dynam.*, *2*, 795–818. doi: 10.5194/wcd-2-795-2021

Maraun, D., M., W., & J.M., G. (2017). Statistical downscaling skill under present climate conditions: A synthesis of the value perfect predictor experiment. *Int J Climatol.*, *39*, 3692-3703. doi: 10.1002/joc.5877

Martius, O., Pfahl, S., & Chevalier, C. (2016). A global quantification of compound precipitation and wind extremes. *Geophysical Research Letters*, *43*(14), 7709-7717. doi: 10.1002/2016GL070017

Montavon, G., Samek, W., & Müller, K.-R. (2018). Methods for interpreting and understanding deep neural networks. *Digital Signal Processing*, *73*, 1-15. doi: 10.1016/j.dsp.2017.10.011

Oktay, O., Schlemper, J., Folgoc, L. L., Lee, M., Heinrich, M., Misawa, K., ... Rueckert, D. (2018). *Attention u-net: Learning where to look for the pancreas.* arXiv. doi: 10.48550/ARXIV.1804.03999

Pan, B., Hsu, K., AghaKouchak, A., & Sorooshian, S. (2019). Improving precipitation estimation using convolutional neural network. *Water Resources Research*, *55*(3), 2301-2321. doi: 10.1029/2018WR024090

Racah, E., Beckham, C., Maharaj, T., Prabhat, & Pal, C. J. (2016). Semi-supervised detection of extreme weather events in large climate datasets. *CoRR*, *abs/1612.02095*. Retrieved from http://arxiv.org/abs/1612.02095

Rasp, S., Dueben, P. D., Scher, S., Weyn, J. A., Mouatadid, S., & Thuerey, N. (2020, Nov). Weatherbench: A benchmark data set for data-driven weather forecasting. *Journal of Advances in Modeling Earth Systems*, *12*(11). doi: 10.1029/2020ms002203

Ronneberger, O., Fischer, P., & Brox, T. (2015). U-Net: Convolutional Networks for Biomedical Image Segmentation. In N. Navab et al. (Eds.), *Medical image computing and computer-assisted intervention – miccai 2015* (pp. 234–241). Springer International Publishing. doi: 10.1007/978-3-319-24574-4_28

Scher, S. (2018). Toward data-driven weather and climate forecasting: Approximating a simple general circulation model with deep learning. *Geophysical Research Letters*, *45* (22), 12,616-12,622. doi: 10.1029/2018GL080704

Schultz, M. G., Betancourt, C., Gong, B., Kleinert, F., Langguth, M., Leufen, L. H., ... Stadtler, S. (2021). Can deep learning beat numerical weather prediction? *Philosophical Transactions of the Royal Society A: Mathematical, Physical and Engineering Sciences*, *379* (2194). doi: 10.1098/rsta.2020.0097

Shi, X. (2020). Enabling smart dynamical downscaling of extreme precipitation events with machine learning. *Geophysical Research Letters*, *47* (19), e2020GL090309. doi: 10.1029/2020GL090309

Shi, X., Chen, Z., Wang, H., Yeung, D., Wong, W., & Woo, W. (2015). Convolutional LSTM network: A machine learning approach for precipitation nowcasting. *CoRR*, *abs/1506.04214*. Retrieved from http://arxiv.org/abs/1506.04214

Shi, X., Gao, Z., Lausen, L., Wang, H., Yeung, D., Wong, W., & Woo, W. (2017). Deep learning for precipitation nowcasting: A benchmark and A new model. *CoRR*, *abs/1706.03458*. Retrieved from http://arxiv.org/abs/1706.03458

Toms, B. A., Barnes, E. A., & Imme, E.-U. (2020). Physically interpretable neural networks for the geosciences: Applications to earth system variability. *Journal of Advances in Modeling Earth Systems*, *12* (9), e2019MS002002. doi: 10.1029/2019MS002002

Trebing, K., Staǹczyk, T., & Mehrkanoon, S. (2021). Smaat-unet: Precipitation nowcasting using a small attention-unet architecture. *Pattern Recognition Letters*, *145*, 178-186. doi: 10.1016/j.patrec.2021.01.036

Trenberth, K., Dai, A., Rasmussen, R. M., & Parsons, D. B. (2003). The changing character of precipitation. *Bull. Am. Meteorol. Soc.*(84), 1205-1218. doi: 10.1175/BAMS-84-9-1205

Vandal, T., Kodra, E., & Ganguly, A. R. (2019). Intercomparison of machine learning methods for statistical downscaling: the case of daily and extreme precipitation. *Theoretical and Applied Climatology*, *137* (1-2), 557–570. doi: 10.1007/s00704-018-2613-3

Weyn, J. A., Durran, D. R., & Caruana, R. (2020). Improving data-driven global weather prediction using deep convolutional neural networks on a cubed sphere. *Journal of Advances in Modeling Earth Systems*, *12* (9), e2020MS002109. doi: 10.1029/2020MS002109

Weyn, J. A., R., D. D., & Caruana, R. (2019). Can machines learn to predict weather? using deep learning to predict gridded 500-hpa geopotential height from historical weather data. *Journal of Advances in Modeling Earth Systems*, *11* (8), 2680-2693. doi: 10.1029/2019MS001705

Wolfensberger, D., Gabella, M., Boscacci, M., Germann, U., & Berne, A. (2021). Rainforest: a random forest algorithm for quantitative precipitation estimation over switzerland. *Atmos. Meas. Tech.*, *14*, 3169–3193. doi: https://doi.org/10.5194/amt-14-3169-2021